TISSUE ENGINEERING: Part A
Volume 25, Numbers 5 and 6, 2019

DOI: 10.1089/ten.tea.2018.0169

termis
Tissue Engineering
& Regenerative Medicine
International Society

ORIGINAL ARTICLE

Nanotechnology Enabled Modulation of Signaling Pathways Affects Physiologic Responses in Intact Vascular Tissue

Kyle M. Hocking, PhD,[1,2] Brian C. Evans, PhD,[1,2] Padmini Komalavilas, PhD,[1,3] Joyce Cheung-Flynn, PhD,[1] Craig L. Duvall, PhD,[2] and Colleen M. Brophy, MD[1,3]

Subarachnoid hemorrhage (SAH) is associated with vasospasm that is refractory to pharmacologic intervention. SAH vasospasm is associated with decreased phosphorylation of intracellular heat shock protein (HSP)20 and increased phosphorylation of HSP27. Phosphorylated HSP20 (p-HSP20) is associated with vascular smooth muscle relaxation and phosphorylated HSP27 with contraction and impaired relaxation. This study was undertaken to modulate these key signaling molecules using intracellular delivery technologies to elucidate the effect of modulation on vasomotor tone of intact vascular tissues. Rat aorta was used as a model system to elucidate the impact of HSP20/HSP27 modulation on physiologic vasomotor responses. HSP20 expression was silenced through siRNA transfection utilizing an endosomolytic diblock copolymer. The diblock copolymer self-assembles into small ($\sim$50 nm) serum stable micellar nanoparticles that effectively package siRNA and facilitate tissue penetration, cell uptake, endosomal escape, intracellular bioavailability, and tissue-level silencing of target gene expression. To increase HSP27 activity, recombinant HSP27 was fused to a cell permeant peptide domain to facilitate protein uptake and activity. Furthermore, a cell permeant peptide mimetic of p-HSP20 was delivered through formulation into nano-polyplexes using a pH-responsive endosomolytic polymer. The impact of these biomolecular modulations on physiologic vasomotor responses in intact tissue was then quantified in a muscle bath. Treatment of rat aorta with HSP20 siRNA polymeric nanocarriers decreased expression of HSP20 which was associated with enhanced contractile responses to phenylephrine (PE) and impaired relaxation responses to sodium nitroprusside. Delivery of recombinant HSP27 to the tissue was associated with increased contractile responses to PE. Treatment with a peptide mimetic of p-HSP20 resulted in decreased contractile responses to PE. These results demonstrate that manipulation of protein levels of the small heat shock phosphoproteins, HSP20 and HSP27, in intact vascular tissues is associated with changes in vasomotor responses. In particular, decreasing HSP20 expression and addition of exogenous HSP27 led to enhanced contractility and impaired relaxation. This biochemical signature is similar to the phenotype of SAH associated vasospasm and suggests that alterations in downstream signaling events may be responsible for SAH induced vasospasm being refractory to upstream, receptor-mediated pharmacologic interventions.

Keywords: subarachnoid hemorrhage, HSP20, HSP27, smooth muscle contraction, nanotechnology, endosomolytic polymer

Impact Statement

Subarachnoid hemorrhage (SAH) is associated with vasospasm that is refractory to traditional vasodilators, and inhibition of vasospasm after SAH remains a large unmet clinical need. SAH causes changes in the phosphorylation state of the small heat shock proteins (HSPs), HSP20 and HSP27, in the vasospastic vessels. In this study, the levels of HSP27 and HSP20 were manipulated using nanotechnology to mimic the intracellular phenotype of SAH-induced vasospasm, and the effect of this manipulation was tested on vasomotor responses in intact tissues. This work provides insight into potential therapeutic targets for the development of more effective treatments for SAH induced vasospasm.

[1]Department of Surgery, Vanderbilt University Medical Center, Nashville, Tennessee.
[2]Department of Biomedical Engineering, Vanderbilt University, Nashville, Tennessee.
[3]VA Tennessee Valley Healthcare System, Nashville, Tennessee.

Introduction

Subarachnoid hemorrhages (SAHs) affect 30,000 people each year and account for 1–7% of all strokes.[1] Bleeding in the subarachnoid space results in the release of oxyhemoglobin that causes prolonged smooth muscle contraction commonly referred to as delayed vasospasm. Delayed vasospasm of cerebral arteries results in delayed onset of ischemic neurological deficits. Arterial vasospasm typically appears 3–4 days after aneurysmal rupture and reaches a peak in severity around 7–10 days. Ischemic neurological deficits typically begin 4–5 days after SAH and are characterized by the insidious onset of confusion and a decreasing level of consciousness that progresses into focal neurological deficits, infarction, coma, and death. Delayed vasospasm parallels the incidence and time course of ischemic neurological deficits and is the most common cause of morbidity and mortality in patients who suffer SAH.[2] Established vasospasm is refractory to traditional vasodilators, and inhibition of vasospasm after SAH remains a large unmet clinical need.

Vasospasm is sustained contraction of blood vessels that may be due to enhanced contraction or impaired relaxation. The two major filaments of smooth muscle, the thick and thin filaments, are the structural components that modulate tone. Thick filaments are composed of myosin. Smooth muscle myosin is also known as myosin II and has two heavy chains. Myosin contains two types of light chains, myosin light chain (MLC)20 and MLC17, with MLC20 being the regulatory chain that is active in contraction. Thin filaments are composed of actin and actin binding proteins. Actin can be present in either filamentous or globular form. Filamentous actin is the polymer form of actin and enables myosin to attach to actin filaments to initiate contraction. Globular actin is the building blocks that form filamentous actin.

Increases in intracellular calcium concentrations ($[Ca^{2+}]_i$) lead to the activation of MLC kinase and increases in the phosphorylation of MLCs (p-MLCs). These changes are thought to lead to cross-bridge cycling and initiation of smooth muscle contraction. Intracellular calcium is thus critical for the initiation of actomyosin interactions. Cross bridges constitute interaction of the globular heads of the myosin filaments (thick filaments) with actin and actin binding proteins (thin filaments).[3–5] In contrast, increases in intracellular cyclic nucleotide content (cyclic adenosine monophosphate [cAMP] and cyclic guanosine monophosphate [cGMP]) activated cyclic nucleotide-dependent protein kinases (cAMP-dependent protein kinase [PKA] and cGMP-dependent protein kinase [PKG]), resulting in relaxation of agonist precontracted smooth muscles or inhibition of agonist-induced contraction.[6,7]

Downstream from the activation of PKA and PKG is a small heat shock protein (HSP) associated with the disruption of actin polymerization, HSP20. Changes in the phosphorylation state of the small HSPs are of the characteristic features of vasospastic vessels after SAH, namely decreased HSP20 phosphorylation and increased phosphorylation of the closely related HSP27.[8] HSP20 and HSP27 have opposing effects on the regulation of smooth muscle tone through dynamic associations with cytoskeletal elements[9–11] (Fig. 1). HSP20 phosphorylation leads to cofilin activation and the depolymerization of actin, resulting in enhanced vasorelaxation,[9,12] whereas HSP27 phosphorylation releases the actin terminus capping function of HSP27, allowing polymerization of actin and concomitant inhibition of smooth muscle relaxation.[11,13–16]

Through the utilization of novel endosomolytic platforms that enable intracellular delivery of biologics to intact rat aortic vascular smooth muscle tissue, we developed a model to demonstrate a direct relationship between acute regulation of small HSPs and vascular physiology. Protein levels were modulated in intact rat aortic tissue with intracellular delivery of HSP20 siRNA and recombinant HSP27 containing a cell permeant peptide domain to recapitulate the intracellular biochemical features of SAH. To enable target gene knockdown in intact vascular tissue, a diblock copolymer that combines dimethylaminoethyl methacrylate (DMAEMA) as the corona-forming block and a copolymer of DMAEMA, butyl methacrylate (BMA), and propylacrylic acid (PAA) as the core-forming block (D-b-DBP)[17] was utilized to assemble siRNA-loaded micellar nanoparticles (Fig. 2A). The positive charge associated with the tertiary amines present on the DMAEMA corona electrostatically condenses the siRNA, whereas the terpolymer core block enables endosomal membrane disruption triggered by the acidic pH in endolysosomal compartments resulting in intracellular siRNA delivery. This work represents the first use of this system in intact vascular tissue.

To mimic the downstream vasorelaxation-promoting effector protein HSP20, peptidomimetics of phosphorylated HSP20 (p-HSP20) were synthesized with a phosphoserine (serine 16) and a cell permeant peptide domain to facilitate peptide translocation across the cell membrane.[12,18] An endosomolytic nano-polyplex (NP) platform based on the pH-responsive polymer poly(propylacrylic acid) (PPAA) was utilized to enhance peptide uptake, intracellular bioavailability, duration of action, and bioactivity.[19,20] NPs are formulated by simple mixing of the cationic p-HSP20 peptide with the anionic PPAA polymer to form electrostatically complexed nanoparticles or NPs (Fig. 2B). Endosomal escape occurs when the NPs are exposed to endosomal pH below the pK_a of the pendant carboxylate moiety on the PPAA polymer (i.e., $pK_a \sim 6.7$) resulting in transition of the polymer into a hydrophobic globular conformation that results in hydrophobic interactions with lipids in the endosomal membrane facilitating endosomal disruption and cytosolic peptide delivery. The increased cytoplasmic bioavailability afforded by this nano-polyplex platform has previously been shown to increase peptide bioactivity by an order of magnitude both *in vitro* and *ex vivo*.[19]

This study was designed to test the effects of intracellular manipulation of downstream effector phosphoproteins (HSP27 and HSP20) on vasomotor responses in intact tissues. The overall goal was to mimic the intracellular phenotype of SAH-induced vasospasm (increased HSP27 and decreased HSP20 phosphorylation) and elucidate potential therapeutic targets for the development of more effective treatments for SAH induced vasospasm.

Materials and Methods

Procurement of rat aorta smooth muscle and physiologic measurements

Fresh cadaveric rat aortas were isolated immediately from euthanized discarded animals from Vanderbilt University

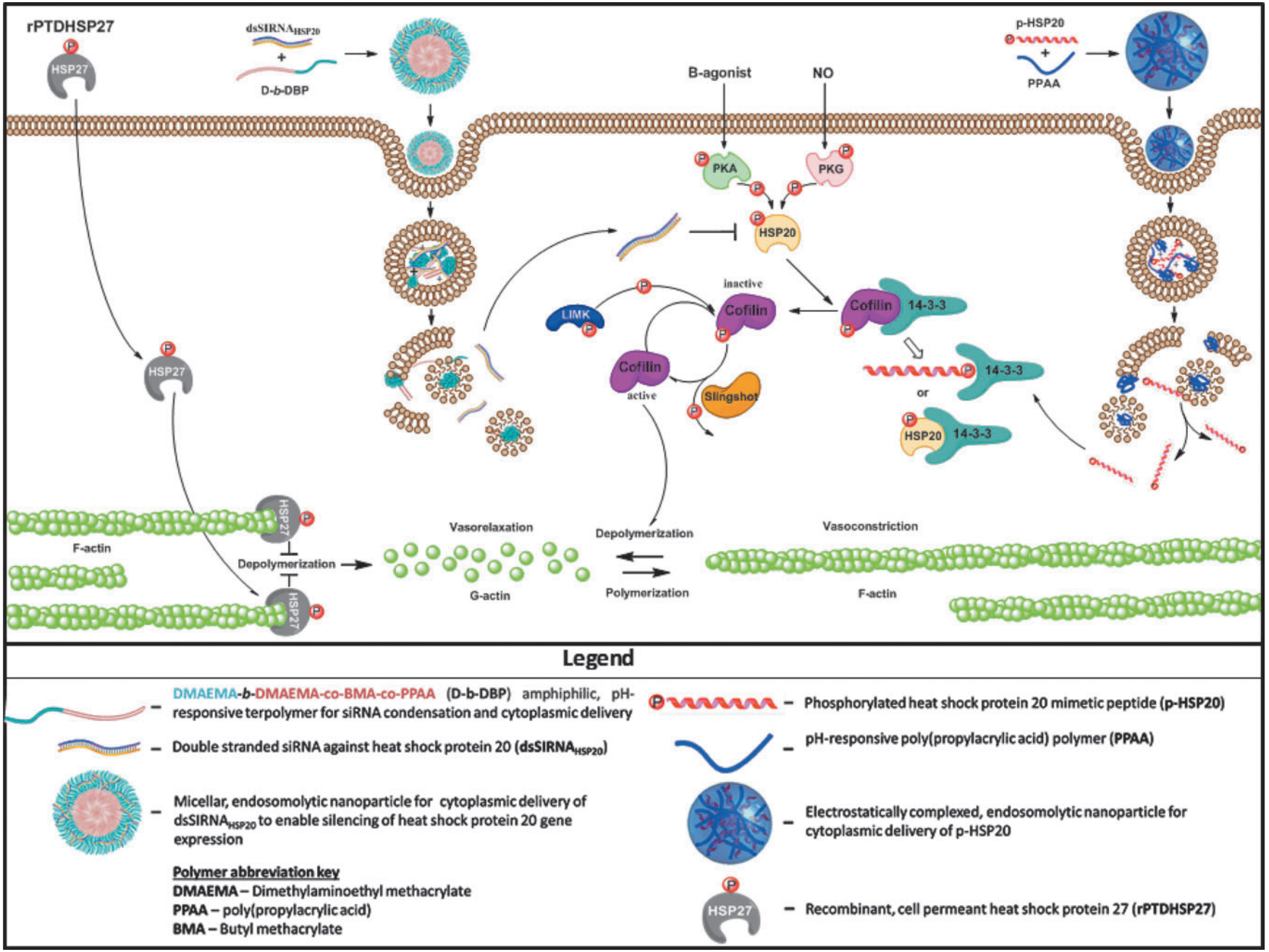

FIG. 1. The influence of HSP27 and HSP20 on actin cytoskeletal dynamics, as well as the involvement of novel endosome-disruptive platforms for the intracellular delivery of biologics. HSP, heat shock protein.

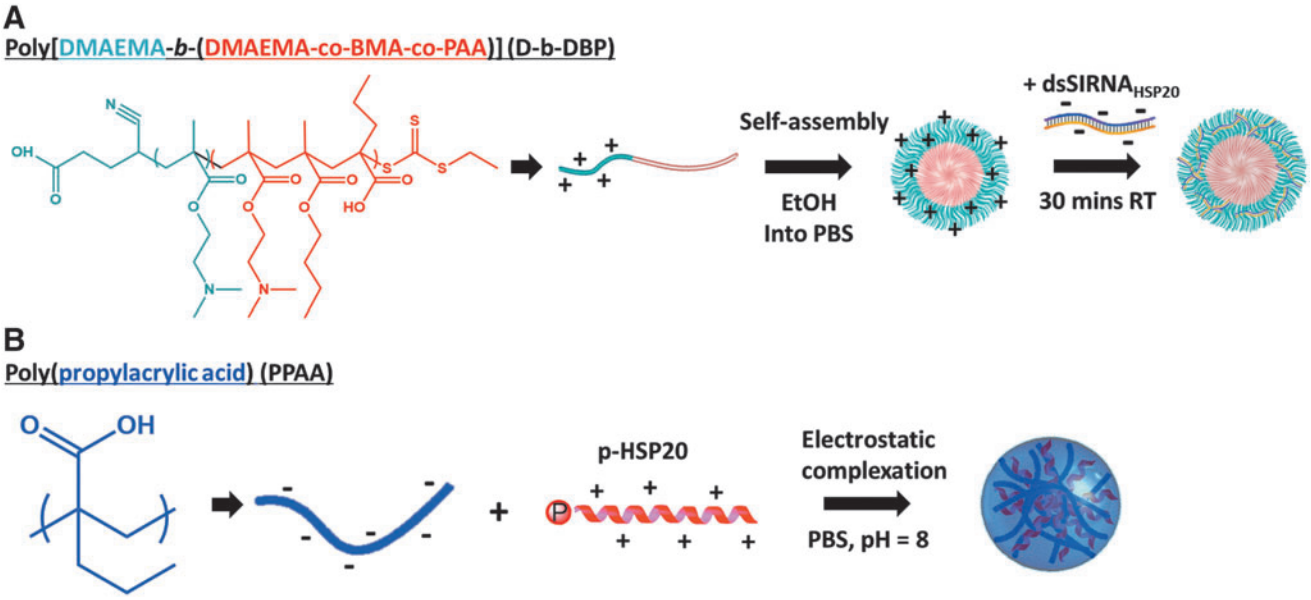

FIG. 2. Assembly of micellar siRNA and electrostatically complexed peptide nanoparticles. **(A)** Micellar nanoparticles were assembled by utilizing our diblock copolymer amphiphile that combines DMAEMA as the corona-forming block and a copolymer of DMAEMA, BMA, and propylacrylic acid (PAA) as the core forming block (D-b-DBP). Nanoparticle self-assembly was induced by dilution from ethanol into PBS, and siRNA was subsequently loaded by electrostatic association. **(B)** Electrostatically complexed peptide nanoparticles were formed by simple mixing of the anionic PPAA polymer and cationic p-HSP20 peptide in pH 8 PBS. BMA, butyl methacrylate; DMAEMA, dimethylaminoethyl methacrylate; PBS, phosphate-buffered saline; PPAA, poly(propylacrylic acid).

Medical Center. All procedures for collection of cadaveric tissue were reviewed and approved by the Vanderbilt University Animal Care and Use Committee. Subcutaneous fat and adventitial tissues were removed, and the vessel was cut into transverse rings of 2.0 mm in width. Rings were suspended in a muscle bath containing a bicarbonate buffer (120 mM NaCl, 4.7 mM KCl, 1.0 mM $MgSO_4$, 1.0 mM NaH_2PO_4, 10 mM glucose, 1.5 mM $CaCl_2$, and 25 mM Na_2HCO_3, pH 7.4), and equilibrated with 95% O_2/5% CO_2, at 37°C. Force measurements were obtained with either a Kent Scientific (Litchfield, CT) force transducer (TRN001) or a Radnoti force transducer (Radnoti Glass Technology, Inc., Monrovia, CA) interfaced with Power Lab from AD Instruments (Colorado Springs, CO) as described earlier.[21] Data were recorded with Chart software, version 5.1.1 (AD Instruments). Rings were washed every 15 min with 37°C bicarbonate buffer for 1 h. The optimal resting tension was determined by progressively stretching the tissue and passively letting the tissue relax. Normally when rat aortic tissue is stretched to 2 g tension, viscoelastic creep returns the force to ~1 g of tension. This process is repeated during equilibration until the resting tension is stabilized and no longer changes upon further stretching. This process was repeated during equilibration until the resting tension stabilized and no longer changed upon further stretching. Rings were manually stretched progressively to the optimal passive stretching tension of 3–4 g and allowed to plateau and maintained at a resting tension of ~1 g for an additional hour as described earlier.[22–25] Rings were then contracted multiple times with high extracellular potassium (110 mM KCl, with equimolar replacement of NaCl in bicarbonate buffer), and the tissue contraction (force) generated was measured. Measured force was normalized for ring weight and length and converted to stress using the formula: stress [10^5Newtons (N)/m^2] = force (g) × 0.0987/area, where area is equal to the wet weight [mg/length (mm at maximal length)] divided by 1.055. The maximal tension obtained was taken as 100%. Rings were equilibrated for an additional 30 min, and dose–response curves for phenylephrine (PE) contraction and sodium nitroprusside (SNP) relaxations were determined to select the correct dose of agents for the experiment. To determine the inhibition of contraction, rings were either treated with buffer alone (control) or p-HSP20 peptide for 30 min. After this, the tissue was contracted again with PE, and inhibition of contraction was measured as % difference in contraction calculated as % maximal depolarization contraction achieved with 110 mM KCl.

Preparation of HSP20 siRNA micelle

Predesigned siRNA was obtained from Invitrogen (Carlsbad, CA) and screened for effectiveness against rat aortic smooth muscle cells with real time polymerase chain reaction (RT-PCR). Once two siRNAs had been selected, they were combined with a diblock copolymer composed of *N*,*N*-DMAEMA, PAA, and BMA synthesized using a reversible addition fragmentation chain transfer polymerization as described previously.[26] Nanoparticles were created by combining 1 mg of the polymeric diblock copolymer with 0.08 mg of siRNA as described previously.[26]

Knockdown of HSP20

The siRNA NPs were added to a HEPES 4-(2-hydroxyethylpiperazine-1-ethanesulfonic acid) buffered Dulbecco's modified Eagle medium (DMEM) at a concentration of 50 nM. Tissue was placed into control, scrambled siRNA

NPs, or HSP20 siRNA NPs. After 24 h of treatment at 37°C, tissue samples were taken out of the DMEM HEPES buffer and placed on the muscle bath apparatus to determine physiologic function as described above where PE (10^{-7} M) was used to contract the tissue and SNP (10^{-9} M) to relax the tissue. At the end of the experiment, tissue samples were frozen for quantification of HSP20 in the tissue.

Construction, purification, and treatment with cell-permeant HSP27 fusion protein

The cDNA encoding human HSP27 was PCR amplified from an I.M.A.G.E (Integrated Analysis of Gene Expression) clone (clone ID 6083486; Clontech, Palo Alto, CA) using a forward primer (5′-GAGCTCATGACCGAGCGCC GCGTC-3′) and a reverse mutagenic primer (5′-GATCGG TACCTTACTTGGCGGCAGTCTCATCGG-3′), then cloned into pCDNA3.1 (Invitrogen), yielding pCDNA3.1-HSP27. Complementary oligonucleotides (5′-ATGGGTGGTTATGC TAGAGCTGCTGCTAGACAAGCTAGAGCTGGTACCG AGCTCCTCGAGG-3′ and 5′-ATCCCTCGAGGAGCTC GGTACCAGCTCTAGCTTGTCTAGCAGCAGCTCTAGC ATAACCACCCA-3′) encoding a protein transduction domain (PTD) were annealed, phosphorylated, and ligated into *Nde*I-*Bam*HI-digested pET14b[27] yielding pET14-bPTD-HSP27. Sequences for all plasmids were confirmed by nucleotide sequence analysis, and protein was expressed in *Escherichia coli* BL21 (DE3; Novagen). Briefly, single colonies of *E. coli* transformed with the pET14b-PTD-plasmid were used to inoculate Luria Broth containing 50 mg/L of ampicillin. Cultures were induced with 2 mM isopropyl-1-thio-β-D-galactopyranoside when the OD_{600} reached 0.6–1. After 3 h, cells were harvested by centrifugation (6000 *g*, 10 min), resuspended in tris-NaCl buffer (100 mM NaCl and 50 mM Tris, pH 8.0), and sonicated on ice. After sonication, the inclusion bodies were harvested by centrifugation (19,000 *g*, 10 min) and resuspended in binding buffer (20 mM Na_2HPO4, 0.5 M NaCl, 50 mM imidazole, pH 7.4). The sample was then added to Ni^{2+}- charged Chelating Sepharose Fast Flow (Pharmacia Biotech, Peapack, NJ) and incubated at room temperature for 30 min. The resin was then washed, and protein was eluted with 300 mM imidazole and dialyzed with phosphate-buffered saline (PBS), pH 8.0 (10 mM Na_2HPO_4, 137 mM NaCl, 27 mM KCL, and 2 mM KH_2PO_4). Rat aortic tissue was treated for 30 min with 15 μM rPTD-HSP27 before being placed on the muscle bath.

Immunoblotting

Proteins from frozen muscle rings were extracted in UDC buffer (8 M urea, 10 mM dithiothreitol, 4% 3-(3-cholamidopropyl)dimethylammonio]-1-propanesulfonate containing protease inhibitor, phosphatase I and II inhibitor cocktail (Sigma, St. Louis, MO)). The mixtures were vortexed at room temperature overnight and then centrifuged at 14,000 rpm for 15 min at 4°C. Soluble protein concentrations were determined using the Bradford assay (Pierce Chemical, Rockford, IL). Equal amounts (20–50 μg) of proteins were placed in a Laemmli sample buffer (Bio-Rad Laboratories, Inc. Hercules, CA), heated for 5 min at 100°C, and separated on sodium dodecyl sulfate-polyacrylamide gels. Proteins from the gels were transferred onto nitrocellulose membranes (Li-COR Biosciences, Lincoln, NE) and blocked before incubation overnight at 4°C with the following primary antibodies: anti-HSP20 (1:3000 dilution, Advanced Immunochemical, Inc., Long Beach, CA), anti-HSP27 (1:2000 dilution; Enzo Life Sciences, Inc., Farmingdale, NY), and anti-GAPDH (1:250; BD Transduction Laboratories). Membranes were washed thrice with tris buffered saline containing Tween 20 (0.1%, TBST) and incubated with appropriate infrared-labeled secondary antibodies (Li-Cor Biosciences) for 1 h at room temperature. The membranes were subsequently washed with TBST, and protein–antibody complexes were visualized and quantified using the Odyssey direct infrared fluorescence imaging system (Li-Cor Biosciences). Data were quantified as the ratio of the HSP20 protein to total GAPDH protein.

Monomer and polymer synthesis

All reagents were purchased from Sigma and were of analytical grade unless otherwise stated. The 2-propylacrylic acid was synthesized according to the procedure outlined by Ferrito *et al.*,[28] utilizing diethyl propylmalonate (Alfa Aesar) as a precursor. The 4-cyano-4-(ethylsulfanylthiocarbonyl) sulfanylpentanoic acid chain transfer agent (CTA) was synthesized as previously described.[17] Reversible addition fragmentation chain transfer polymerization of the PPAA homopolymer was carried out in bulk under a nitrogen atmosphere at 70°C for 48 h using 2,2′-azo-bis-isobutyrylnitrile (AIBN) as the free radical initiator. The reaction mix was put through three freeze-vacuum-thaw cycles and purged with nitrogen for 30 min before polymerization. The molar ratio of CTA to AIBN was 1 to 1, and the monomer to CTA ratio was set so that a degree of polymerization of 190 would be achieved at 100% conversion. Following polymerization, the resultant polymer was dissolved in dimethylformamide (DMF) and precipitated into ether five times before drying overnight *in vacuo*. Gel permeation chromatography (Agilent) was used to determine molecular weight and polydispersity (M_w/M_n, polydispersity index [PDI]) of the PPAA homopolymer using high-performance liquid chromatography (HPLC)-grade DMF containing 0.1% LiBr at 60°C as the mobile phase. Molecular weight calculations were performed with ASTRA V software (Wyatt Technology) and were based on experimentally determined dn/dC values determined through offline injections of the polymer through a refractive index detector [$M_n = 22{,}292$ (g/mol), PDI = 1.471, dn/dC = 0.087 (mL/g)].

Polyplex

The HSP20 phosphopeptide was synthesized using solid phase synthesis and purified by HPLC as verified through electrospray-ionization mass spectrometry. NPs were formed by simple mixing of the PPAA homopolymer with the HSP20 phosphopeptide in PBS at pH 8.0, which is between the pK_a values of the primary amines present on the HSP20 phosphopeptide and the carboxylic acids on PPAA; this condition ensures optimal solubility and net charge on both molecules. The PPAA polymer was chosen because of its well defined pH-dependent membrane disruptive activity that has been shown to facilitate endosomal escape[29–31] and successful use in animal models.[32–34]

To determine optimal nanoparticle formulation conditions, a library of pHSP20-NPs was prepared at various charge

ratios (i.e., charge ratio $[CR] = ([NH_3^+]_{MK2i}/[COO^-]_{PPAA})$ from 10:1 to 1:10, and the size distribution and particle surface charge were characterized through dynamic light scattering and ζ-potential analysis, respectively. As expected, pHSP20-NP ζ-potential was directly proportional to the CR, with an apparent isoelectric CR ~3:1. Charge ratio was found to significantly affect pHSP20-NP size and charge, with a CR = 3:1 yielding a unimodal size distribution. A CR of 1:3 was chosen as the optimal formulation as this ratio consistently yielded a unimodal size distribution with minimal particle size and polydispersity ($d_h = 240.9 \pm 15.51$ nm, $\zeta = -0.91 \pm 2.56$ mV). It is hypothesized that at the lower pH, the PPAA polymer becomes protonated/deionized, and the net positive charge on the peptide causes electrostatic repulsion and disassembly of the pHSP20-NPs. This effect releases the therapeutic payload and ensures that peptide bioactivity is not sterically hindered by NP encapsulation.

Cytosolic Ca^{2+} measurements

Rings of rat aorta were suspended on hooks in a FluoroPlex Tissue Bath Fluorometry System (IonOptix LLC, Milton, MA and Radnoti Glass Technology, Inc., Monrovia, CA), which enables fluorescence ion recording in parallel with force measurement. Force measurements were obtained with a Radnoti force transducer (Radnoti Glass Technology, Inc.) interfaced with Power Lab from AD Instruments (Colorado Springs) as described earlier.[21] Rings were loaded at room temperature with 10 μM Fura-2 AM ester and 0.01% Pluronic F-127 in the bicarbonate buffer for 4 h. After loading, rings were washed every 10 min with 37°C bicarbonate buffer for 1 h. Calcium flux was measured with optical fibers that were interfaced with Power Lab. Fluorescence was measured at both 380 and 340 nm of wavelength, simultaneously. The ratio of the emission of the two wavelengths was used to determine intracellular changes in calcium concentration. Baseline ratio was set at 1.0, and changes in this ratio in response to stimuli were measured. Baseline calcium fluorescence was measured, and the background was set to zero as an output of 1 volt. To determine the inhibition of contraction, rings were either treated with control or HSP20 phosphopeptidomimetic (p-HSP20). The tissue was then challenged with PE, and the % inhibition of contraction and calcium concentrations were measured. To add PE while continuously measuring intracellular calcium concentrations, an infusion line filled with bicarbonate buffer was used to keep the system in a closed light impenetrable state. The amount of buffer in the infusion line was adjusted to achieve the final concentration of the agonist in the bath. Force and calcium fluorescence were measured continuously for 15 min after the addition of PE.

Actin assay

The amount of F-actin versus total actin (F-actin/[F-actin + G-actin]) was measured using the G-actin/F-actin In Vivo Assay Kit (Cytoskeleton, Denver, CO), as per manufacturer's protocol as described earlier.[21] Briefly, treated rat aortic samples were homogenized in 1 mL of lysis buffer (50 mM PIPES pH 6.9, 50 mM NaCl, 5 mM $MgCl_2$, 5 mM EGTA, 5% (v/v) Glycerol, 0.1% Nonidet P40, 0.1% Triton X-100, 0.1% Tween 20, 0.1% 2-mercapto-ethanol, 0.001% Antifoam C, 4 μM Tosyl arginine methyl ester, 15 μM Leupeptin, 10 μM Pepstatin A, 10 mM Benzamidine, and 1 mM ATP warmed to 37°C) for 1 min with a mortar and pestle that fit into a 1.5 mL microfuge tube. The lysate was centrifuged at 2000 rpm for 5 min at 37°C to pellet unbroken cells. The supernatants were centrifuged at $100{,}000 \times g$ for 1 h at 37°C. Supernatants (contain the G-actin) were transferred to precooled tubes and placed on ice. The pellets (contain F-actin) were resuspended in 1 mL of ice-cold 10 μM cytochalasin D in deionized water, and F-actin was depolymerized by incubating for 1 h on ice with mixing every 15 min. Equal volume of supernatants and pellets along with actin standards (2–20 μg) was separated on 12% SDS-polyacrylamide gels and transferred to nitrocellulose membrane in 1X Tris-Glycine buffer at 100 volts for 1 h. The membrane was probed with anti-actin antibody, and the amount of actin in each fraction was quantified comparing to actin standards loaded on the same gel.

Data analysis

Data are reported as mean responses ± standard error of the mean. Paired *t*-tests are used for Figure 4, and one-way ANOVA analyses were conducted for Figures 3, 5, and 6 to determine the significance (p-value) of each experiment. A *p*-value <0.05 was considered statistically significant.

Results

HSP20 gene silencing and smooth muscle physiology

The effect of downregulation of downstream effector phosphoprotein HSP20 on vasomotor responses in intact tissues was examined by silencing the HSP20 gene using siRNA. HSP20 gene silencing was confirmed at the protein level using western blot techniques to quantify tissue HSP20 levels normalized to tissue GAPDH levels. Tissue treated with HSP20 siRNA led to a significantly lower amount of HSP20/GAPDH (0.16 ± 0.02 A.U.) than control (0.50 ± 0.21 A.U.) or scrambled siRNA groups (0.46 ± 0.16 A.U.) ($p < 0.05$, $n = 6$, Fig. 3A), demonstrating that siRNA transfection using an endosomolytic polymeric micelle successfully silences HSP20 expression in intact tissue *ex vivo*.

The effect of HSP20 knockdown on the physiologic response of the rat aorta was determined in the muscle bath. Contraction to 10^{-7} M PE of control (47% ± 5.7%) and scrambled siRNA (46% ± 6.6%) treated aorta was significantly ($p < 0.01$, $n = 5$) lower compared with rat aorta treated with HSP20 siRNA (59% ± 7.3%) ($p < 0.05$, $n = 6$, Fig. 3B). In addition, tissue treated with HSP20 siRNA demonstrated significantly lower relaxation (58% ± 4.9%) to 10^{-9} M SNP compared to untreated control (84% ± 3.5%) and scrambled siRNA (83% ± 3.0%) treated tissue ($p < 0.01$, $n = 5$; Fig. 3C, D).

rPTD-HSP27 and its effect on smooth muscle

To test the effect of increasing the concentration of HSP27 on smooth muscle contractility, rat aortic segments were treated with a recombinant cell permeant HSP27 fusion protein (rPTD-HSP27). To ensure that intracellular HSP27 was increased by this approach, western blot techniques were used to compare HSP27 levels with β-actin. Tissue treated with rPTD-HSP27 had a significantly greater ratio of HSP27/β-actin than untreated control tissues (Fig. 4A). Rat aortic tissue treated with rPTD-HSP27 yielded significantly

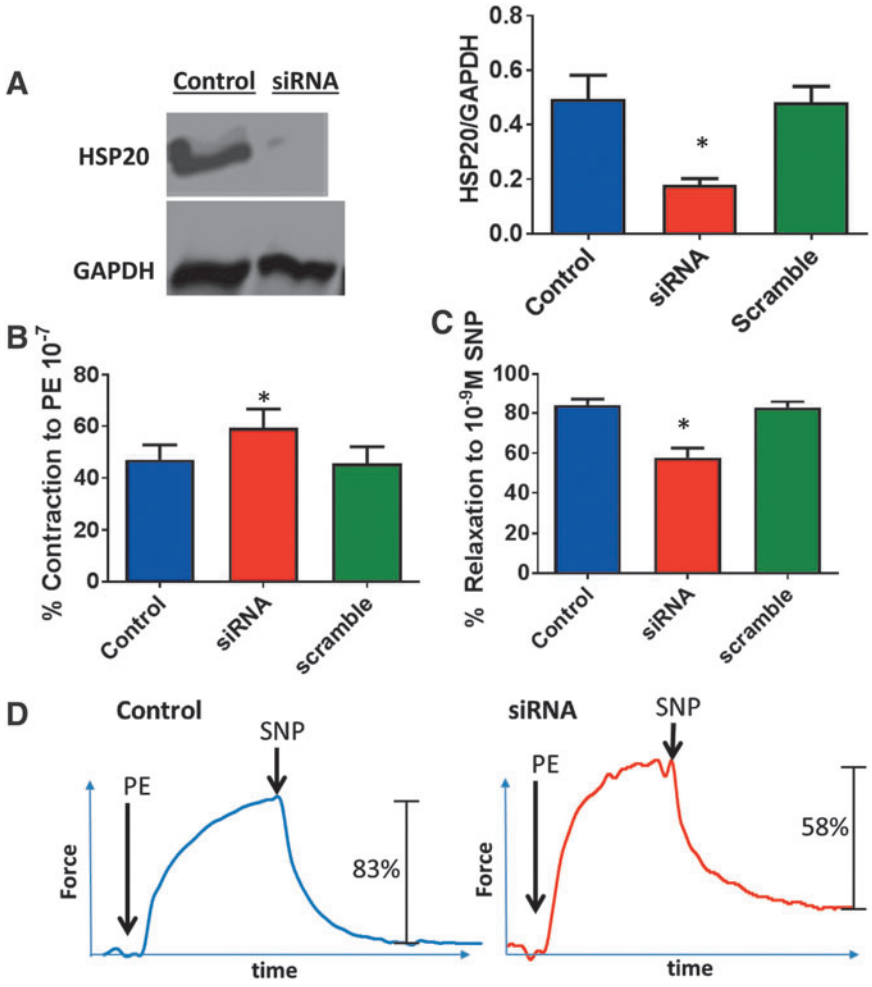

FIG. 3. HSP20 gene silencing and smooth muscle physiology. HSP20 siRNA was loaded into the D-DBP diblock copolymer nanoparticles. Rat aortic tissue was untreated (control), treated with scrambled siRNA nanoplexes (50 nM, Scramble), or HSP20 siRNA nanoplexes (50 nM, siRNA) for 24 h at 37°C and placed on the muscle bath, contracted with PE (10^{-7} M) and relaxed with SNP (10^{-9} M). Panel **(A)**, representative western blot and cumulative data of HSP20 expression. Tissue treated with HSP20 siRNA showing significantly lower amount of HSP20/GAPDH than control or scrambled siRNA groups. Panel **(B)**, contraction of siRNA treated tissue. Contraction to PE of control and scrambled siRNA treated aorta was significantly lower compared with rat aorta treated with HSP20 siRNA. Panel **(C)**, relaxation of siRNA treated tissue to SNP. Relaxation of HSP20 siRNA treated tissue was significantly lower than control or scrambled siRNA treated tissue. For **(A–C)**, $*p \leq 0.05$, $n \geq 5$ (one-way ANOVA). Panel **(D)**, Representative tracing of contraction with PE and relaxation with SNP of scramble and HSP20 siRNA treated tissue. Statistical significance was determined with a one-way ANOVA. ANOVA, analysis of variance; PE, phenylephrine; SNP, sodium nitroprusside.

lower vasorelaxation to 10^{-9} M SNP than control tissue in a muscle bath (60% ± 7% vs. 82% ± 11% relaxation, respectively; $p < 0.05$, $n = 4$, Fig. 4B, C).

p-HSP20 peptide mediated inhibition of contraction

A peptide mimetic of p-HSP20 was delivered to rat aortic smooth muscle before PE challenge to assess the vasoactive effects of HSP20 phosphorylation. To assess the influence of enhanced cytoplasmic peptide delivery, p-HSP20 was formulated into an endosomolytic NP delivery system to compare the delivery of the peptide alone (100, 500, and 1000 μM doses of the peptide alone and 100, 200, and 500 μM doses of the NP formulations). Percent inhibition of contraction was utilized to determine the effect of the peptide on smooth muscle physiology (Fig. 5A). Control segments displayed significantly less inhibition of contraction than all other groups (−2.4% ± 1.8%; $p < 0.0001$, $n = 4$–6; Fig. 5B). Treatment with 100 μM p-HSP20 alone displayed significantly less inhibition than an equivalent dose of peptide delivered through the NP formulation (16.5% ± 1.3% vs. 36.8% ± 4.9%, respectively). Similarly, treatment with 500 μM p-HSP20 displayed significantly less% inhibition than 500 μM p-HSP20-NPs (37.1% ± 5.3% vs. 95.7% ± 1.6%, respectively). Treatment with 200 μM p-HSP20-NPs resulted in an equivalent inhibition of contraction as a 1 mM dose of the free p-HSP20 peptide, indicating a fivefold increase in peptide mediated bioactivity when delivered through the endosomolytic NP formulation. Both p-HSP20 and p-HSP20-NP treatment showed a dose-dependent increase in inhibition of contraction in rat aortic tissue.

Intracellular calcium changes during inhibition of contraction

While calcium modulation has been implicated in the regulation of smooth muscle tone, the small HSPs function as direct cytoskeletal regulators.[35] To determine if inhibition of contraction by p-HSP20 is independent of changes in intracellular calcium concentration, rat aorta was suspended in a Fluoroplex apparatus. Control segments displayed significantly lower inhibition of contraction (−2.4% ± 1.8%; $p < 0.05$, $n = 4$, Fig. 5B) compared with tissue treated with 500 μM p-HSP20-NPs (95.7% ± 1.6%). However, no difference was observed in the rise in intracellular calcium concentrations between untreated control and p-HSP20-NP treated tissue (171.4 ± 23.0 nM $[Ca^{2+}]_i$ vs. 172.6 ± 27.3 nM $[Ca^{2+}]_i$, respectively; Fig. 5C, D) following the addition of 10^{-7} M PE to induce contraction. These results verify that the enhanced inhibition of contraction seen in p-HSP20-NP treated tissue is independent of intracellular calcium transients and is mediated by increased cytoplasmic bioavailability of the p-HSP20 peptide and not by the pH-responsive PPAA polymer acting as a calcium chelator.

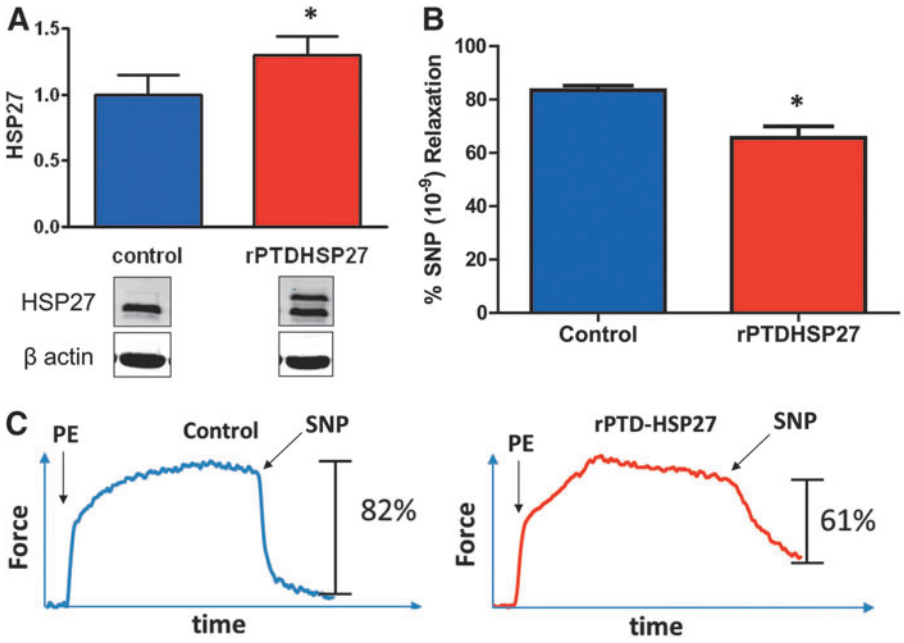

FIG. 4. Effect of rPTD-HSP27 delivery on smooth muscle contractility. Rat aortic tissue was treated with buffer (control) or rPTD-HSP27 (15 μM) for 30 min, expression was determined by western blotting, and relaxation to SNP was determined in a muscle bath. **(A)** Cumulative data and representative blot showing protein levels of HSP27. **(B)** Cumulative graph showing SNP-induced relaxation of rPTD-HSP27 treated rat aortic tissue. **(C)** Representative tracing of SNP-induced relaxation. Tissue treated with rPTD-HSP27 had a significant decrease in SNP (10^{-9} M)-induced vasorelaxation. $*p \leq 0.05$, $n = 4$ (paired t-test).

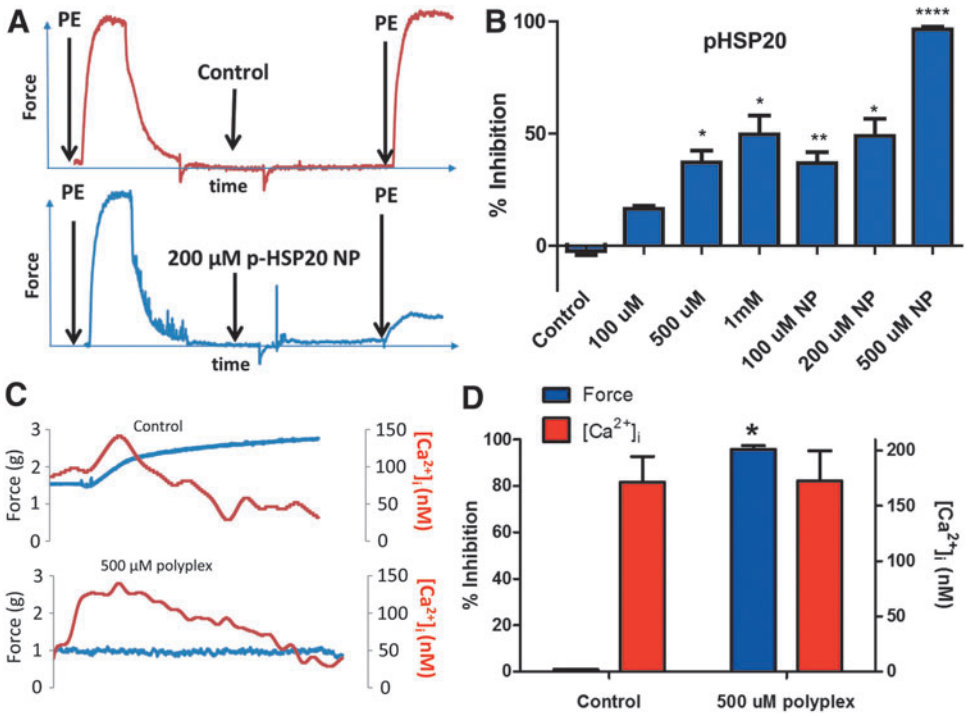

FIG. 5. Endosomolytic nanoplex delivery system enhances the delivery of p-HSP20 and inhibition of contraction. Rings of rat aorta were suspended in a FluoroPlex Tissue Bath Fluorometry System that can measure contraction and intracellular calcium concentration simultaneously. Rings were untreated (control), treated with different doses of the p-HSP20 peptide alone (100, 500, and 1000 μM), or peptide-nanoplex formulations (100, 200, and 500 μM), and inhibition of contraction and calcium concentration were measured. **(A)** Representative tracing showing contraction with PE and inhibition of contraction with p-HSP20 NP. **(B)** Cumulative data demonstrating enhanced inhibition of contraction with p-HSP20 or p-HSP20 NP. **(C)** Representative tracing showing inhibition of contraction and intracellular calcium concentration with 500 μM p-HSP20 NP (500 μM polyplex). **(D)** Cumulative data showing percent inhibition of contraction (force) and intracellular calcium concentration ($[Ca^{2+}]_i$). A fivefold increase in peptide mediated bioactivity was observed when delivered through the endosomolytic NP formulation compared to peptide alone without any change in the $[Ca^{2+}]_i$. $*p<0.05$, $**p<0.001$, $****p<0.00001$, $n = 4$–6 (one-way ANOVA). p-HSP20 NP, p-HSP20 nanoplex.

Actin polymerization

Since both HSP20 and HSP27 affect actin cytoskeletal dynamics, the effect of manipulation of the levels of these proteins on actin cytoskeleton was examined in intact rat aorta. Actin polymerization was analyzed to elucidate how acute modulation of small HSP signaling affects actin cytoskeletal dynamics in intact vascular tissue. Filamentous actin (F) was compared to globular actin (G) in rat aortic tissue that was isolated through ultracentrifugation of tissue homogenates. Silencing HSP20 expression in rat aorta significantly increased F-actin polymerization (41% ± 2.9% F-actin), whereas treatment with 1 mM p-HSP20 peptide significantly reduced the amount of F-actin (15% ± 1.2%) compared to control tissue (24% ± 2.3%) (Fig. 6). Treatment with rPTD-HSP27 significantly increased F-actin (30% ± 1.4%) compared to control tissue (Fig. 6).

Discussion

SAH-induced vasospasm is uniquely refractory to receptor mediated pharmacologic intervention. We hypothesized that this may be due, in part, to changes in the expression and phosphorylation of downstream effector proteins, specifically the small HSPs HSP20 and HSP27 that regulate cytoskeletal dynamics to modulate vascular tone. To test this hypothesis, the intracellular levels of the small HSPs were modulated in intact rat aortic tissue utilizing a variety of novel intracellular delivery systems to recapitulate the vasospastic vascular phenotype characteristic of SAH and as a therapeutic approach to treat pathological vasoconstriction.

HSP20 gene silencing was achieved in rat aortic tissue using siRNA delivered through an endosomolytic micellar nanoparticle. Downregulation of HSP20 was associated with increased PE-induced contraction and decreased SNP-induced relaxation. Typically, genetic modulation of protein expression in intact vascular tissue is problematic due to low delivery efficiency and low protein turnover compared to cultured cells. However, the use of pH-responsive nanoparticles[17,26] was shown to enhance siRNA intracellular bioavailability resulting in enhanced gene silencing and leading to functional changes in intact vascular tissue within 24 h.

A recombinant HSP27 protein was generated that contained a protein transduction domain to produce increases in intracellular concentrations of HSP27. Increasing intracellular levels of HSP27 also produced a phenotype in which SNP induced relaxation was impaired. Conditions were not modified to reduce HSP27 expression in rat aorta in that basal levels of HSP27 in rat aorta are very low (Fig. 4A). Thus, both decreasing the expression of HSP20 and increasing the expression of HSP27 led to decreased relaxation responses to SNP.

Decreasing the expression of HSP20 or increasing the expression of HSP27 both led to increases in the polymerization of F-actin. Thin filament regulation through alterations in the ratio of G- (globular) to F- (filamentous) actin modulates vascular tone by providing scaffolding for the regulatory myosin heavy chains and the myosin motor.[21,36,37]

To produce a therapeutic relaxation response by modulating downstream effector responses, a peptide mimetic of p-HSP20 was delivered through an endosomolytic NP formulation. Treatment with p-HSP20 led to inhibition of PE induced vasoconstriction in rat aortic tissue. In this instance, inhibition of contraction was used as a surrogate for vasorelaxation.[21] The NP formulation was utilized to facilitate endosomal escape through the pH-dependent membrane disruptive activity of PPAA, allowing for increased therapeutic bioactivity at a lower dose of p-HSP20 peptide. There was a dose dependent inhibition of contraction with p-HSP20 treatment and a roughly fivefold increase in inhibition of contraction when the peptide was delivered through the NP formulation. These data further suggest that phosphorylation of HSP20 on Ser[16] results in relaxation of smooth muscle and that cytosolic peptide delivery using endosomolytic nanoparticles significantly enhanced p-HSP20

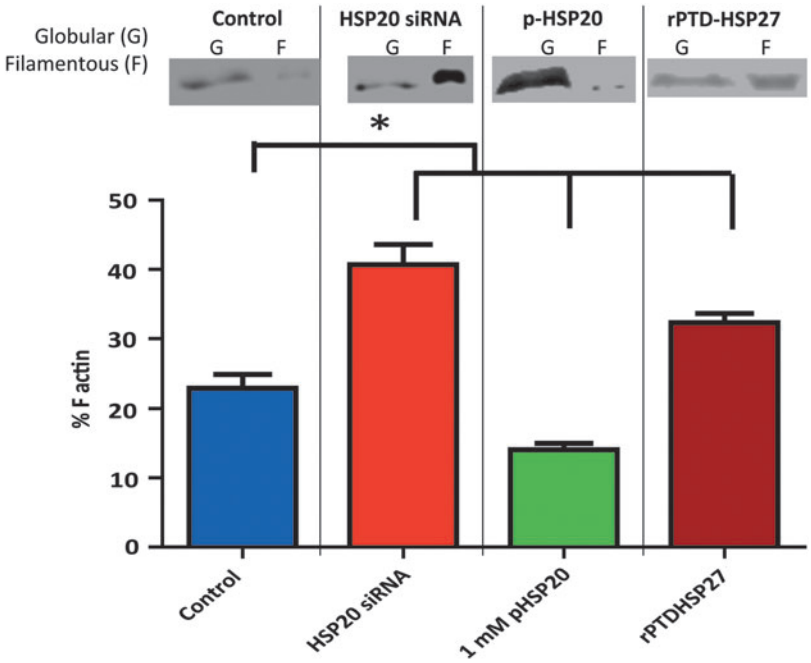

FIG. 6. Silencing HSP20 expression and treatment with pHSP20 or rPTD-HSP27 affects actin polymerization in rat aorta. Rat aortic segments were untreated (control), treated with HSP20 siRNA (50 nM) nanoplexes for 24 h, p-HSP20 peptide (1 mM, 30 min), or rPTD-HSP27 (15 μM, 30 min), and then the amount of F-actin versus total actin (F-actin + G-actin) was measured using the G-actin/F-actin In Vivo Assay Kit. Silencing HSP20 expression or treatment with rPTD-HSP27 significantly increased F-actin polymerization, whereas treatment with 1 mM p-HSP20 peptide significantly reduced the amount of F-actin compared to control tissue. *$p \leq 0.05$, $n = 4$ (one-way ANOVA).

bioactivity. Due to the delayed onset of spasm in patients with SAH, treatment with a downstream mimetics such as the p-HSP20 peptide could be used to prevent or treat symptomatic vasospasm following SAH.

The p-HSP20 and p-HSP20-NPs were able to inhibit force generation independent of rises in intracellular calcium, suggesting that the relaxation induced by these peptide mimetics was independent of calcium signaling and more likely related to the observed alterations in actin filament dynamics.[21] This finding holds clinically significant implications for treatment of SAH induced vasospasm as mean arterial blood pressure would not be as greatly impacted if intracellular calcium signaling remains unchanged following treatment. To this end, previous work has confirmed that p-HSP20 does not affect mean arterial pressure in a mouse model.[38]

This vascular physiology model using novel delivery systems for manipulation of intracellular phenotype provides insight into why SAH-induced vasospasm is refractory to typical pharmacologic approaches. A decrease in the amount and/or phosphorylation of downstream HSP20 protein renders upstream pharmacologic NO-donors such as SNP ineffective. In addition, since calcium independent cytoskeletal regulators are implicated in symptomatic vasospasm, the use of calcium channel blockers would be nonspecific and ineffective. In addition to providing these insights into the biomolecular events underlying pathological vasoconstriction, this model also identifies novel therapeutic approaches in directly manipulating these downstream cytoskeletal modulators for the treatment of pathological vasoconstriction such as symptomatic vasospasm following SAH.

The major limitation of this study is the use of rat aortic tissue as opposed to human artery. Rat aorta was used because it has more consistency in HSP levels and because it has substantially less variability in physiologic muscle bath studies than human samples typically acquired from our center. Future studies should include manipulation of HSPs in human cerebrovascular tissue and translation of these results into *in vivo* models of SAH-induced vasospasm.

Conclusions

siRNA mediated silencing of HSP20 expression and intracellular delivery of recombinant HSP27 were used to reproduce a biomolecular phenotype in normal arterial tissue similar to that found in pathologic vasospastic vessels following SAH. Decreases in the expression of HSP20 and increases in the intracellular levels of HSP27 enhanced agonist-induced vasoconstriction and decreased vasorelaxation in response to nitrovasodilators consistent with vasospasm.

Changes in the expression and/or phosphorylation of the small HSPs, HSP20 and HSP27, represent one of the mechanisms by which calcium independent signaling modulates vasomotor tone. Thus, modulating the activity of these small HSPs represents a promising highly specific approach to both model and treat SAH induced vasospasm. Furthermore, since these small HSPs act independently of changes in intracellular calcium concentrations and are downstream of receptor mediated signaling pathways, targeting p-HSP20 and HSP27 should specifically modulate SAH-induced vasospastic vessels while circumventing systemic hypotension. Taken together, this work provides insight into novel calcium independent mechanisms of smooth muscle tone regulation and highlights new therapeutic approaches to more specifically and effectively treat SAH induced symptomatic vasospasm.

Acknowledgments

This study was supported, in part, by NIH grants RO1HL70715 to C.M.B. and R01 EB019409 and R01 HL122347 to C.L.D.

Disclosure Statement

No competing financial interests exist.

References

1. Harrod, C.G., Bendok, B.R., and Batjer, H.H. Prediction of cerebral vasospasm in patients presenting with aneurysmal subarachnoid hemorrhage: a review. Neurosurgery **56,** 633, 2005.
2. Lee, K.H., Lukovits, T., and Friedman, J.A. ''Triple-H'' therapy for cerebral vasospasm following subarachnoid hemorrhage. Neurocrit Care **4,** 68, 2006.
3. Horowitz, A., Menice, C.B., Laporte, R., and Morgan, K.G. Mechanisms of smooth muscle contraction. Physiol Rev **76,** 967, 1996.
4. Kamm, K.E., and Stull, J.T. The function of myosin and myosin light chain kinase phosphorylation in smooth muscle. Annu Rev Pharmacol Toxicol **25,** 593, 1985.
5. Murphy, R.A., and Rembold, C.M. The latch-bridge hypothesis of smooth muscle contraction. Can J Physiol Pharmacol **83,** 857, 2005.
6. Lincoln, T.M. cGMP and mechanisms of vasodilation. Pharm Ther **41,** 479, 1989.
7. Murray, K.J. Cyclic AMP and mechanisms of vasodilation. Pharmacol Ther **47,** 329, 1990.
8. Macomson, S.D., Brophy, C.M., Miller, W., Harris, V.A., and Shaver, E.G. Heat shock protein expression in cerebral vessels after subarachnoid hemorrhage. Neurosurgery **51,** 204, 2002.
9. Dreiza, C.M., Brophy, C.M., Komalavilas, P., *et al.* Transducible heat shock protein 20 (HSP20) phosphopeptide alters cytoskeletal dynamics. FASEB J **19,** 261, 2005.
10. Dreiza, C.M., Komalavilas, P., Furnish, E.J., *et al.* The small heat shock protein, HSPB6, in muscle function and disease. Cell Stress Chaperones **15,** 1, 2010.
11. Gerthoffer, W.T., and Gunst, S.J. Invited review: focal adhesion and small heat shock proteins in the regulation of actin remodeling and contractility in smooth muscle. J Appl Physiol (1985) **91,** 963, 2001.
12. Flynn, C.R., Komalavilas, P., Tessier, D., *et al.* Transduction of biologically active motifs of the small heat shock-related protein, HSP20, leads to relaxation of vascular smooth muscle. Faseb J **17,** 1358, 2003.
13. Dubińska-Magiera, M., Jabłońska, J., Saczko, J., Kulbacka, J., Jagla, T., and Daczewska, M. Contribution of small heat shock proteins to muscle development and function. FEBS Lett **588,** 517, 2014.
14. Wettstein, G., Bellaye, P.S., Micheau, O., and Bonniaud, P. Small heat shock proteins and the cytoskeleton: an essential interplay for cell integrity? Int J Biochem Cell Biol **44,** 1680, 2012.
15. An, S.S., Fabry, B., Mellema, M., *et al.* Role of heat shock protein 27 in cytoskeletal remodeling of the airway smooth muscle cell. J Appl Physiol (1985) **96,** 1701, 2004.

16. Yamboliev, I.A., Hedges, J.C., Mutnick, J.L., Adam, L.P., and Gerthoffer, W.T. Evidence for modulation of smooth muscle force by the p38 MAP kinase/HSP27 pathway. Am J Physiol Heart Circ Physiol **278,** H1899, 2000.
17. Convertine, A.J., Benoit, D.S., Duvall, C.L., Hoffman, A.S., and Stayton, P.S. Development of a novel endosomolytic diblock copolymer for siRNA delivery. J Control Release **133,** 221, 2009.
18. Lopes, L.B., Furnish, E.J., Komalavilas, P., *et al.* Cell permeant peptide analogues of the small heat shock protein, HSP20, reduce TGF-beta1-induced CTGF expression in keloid fibroblasts. J Invest Dermatol **129,** 590, 2009.
19. Evans, B.C., Hocking, K.M., Kilchrist, K.V., Wise, E.S., Brophy, C.M., and Duvall, C.L. Endosomolytic nano-polyplex platform technology for cytosolic peptide delivery to inhibit pathological vasoconstriction. ACS Nano **9,** 5893, 2015.
20. Evans, B.C., Hocking, K.M., Osgood, M.J., *et al.* MK2 inhibitory peptide delivered in nanopolyplexes prevents vascular graft intimal hyperplasia. Sci Transl Med **7,** 291ra95, 2015.
21. Hocking, K.M., Baudenbacher, F.J., Putumbaka, G., *et al.* Role of cyclic nucleotide-dependent actin cytoskeletal dynamics:Ca(2+)](i) and force suppression in forskolin-pretreated porcine coronary arteries. PLoS One 8**,** e60986, 2013.
22. Jespersen, B., Tykocki, N.R., Watts, S.W., and Cobbett, P.J. Measurement of smooth muscle function in the isolated tissue bath-applications to pharmacology research. J Vis Exp 52324, 2015.
23. Bai, T.R., Bates, J.H., Brusasco, V., *et al.* On the terminology for describing the length-force relationship and its changes in airway smooth muscle. J Appl Physiol (1985) **97,** 2029, 2004.
24. Hocking, K.M., Brophy, C., Rizvi, S.Z., *et al.* Detrimental effects of mechanical stretch on smooth muscle function in saphenous veins. J Vasc Surg **53,** 454, 2011.
25. Herlihy, J.T., and Murphy, R.A. Length-tension relationship of smooth muscle of the hog carotid artery. Circ Res **33,** 275, 1973.
26. Nelson, C.E., Kim, A.J., Adolph, E.J., *et al.* Tunable delivery of siRNA from a biodegradable scaffold to promote angiogenesis in vivo. Adv Mater **26,** 607, 2014.
27. Lopes, L.B., Brophy, C.M., Flynn, C.R., *et al.* A novel cell permeant peptide inhibitor of MAPKAP kinase II inhibits intimal hyperplasia in a human saphenous vein organ culture model. J Vasc Surg **52,** 1596, 2010.
28. Ferrito, M.S., and Tirrell, D.A. Poly(2-ethylacrylic acid). In: Macromolecular Syntheses. Vol. 11, New York, NY: Wiley, 1992, pp. 59-62.
29. Jones, R.A., Cheung, C.Y., Black, F.E., *et al.* Poly(2-alkylacrylic acid) polymers deliver molecules to the cytosol by pH-sensitive disruption of endosomal vesicles. Biochem J **372,** 65, 2003.
30. Lackey, C.A., Press, O.W., Hoffman, A.S., and Stayton, P.S. A biomimetic pH-responsive polymer directs endosomal release and intracellular delivery of an endocytosed antibody complex. Bioconjug Chem **13,** 996, 2002.
31. Murthy, N., Robichaud, J.R., Tirrell, D.A., Stayton, P.S., and Hoffman, A.S. The design and synthesis of polymers for eukaryotic membrane disruption. J Control Release **61,** 137, 1999.
32. Foster, S., Duvall, C.L., Crownover, E.F., Hoffman, A.S., and Stayton, P.S. Intracellular delivery of a protein antigen with an endosomal-releasing polymer enhances CD8 T-cell production and prophylactic vaccine efficacy. Bioconjug Chem **21,** 2205, 2010.
33. Murthy, N., Campbell, J., Fausto, N., Hoffman, A.S., and Stayton, P.S. Bioinspired pH-responsive polymers for the intracellular delivery of biomolecular drugs. Bioconjug Chem **14,** 412, 2003.
34. Crownover, E., Duvall, C.L., Convertine, A., Hoffman, A.S., and Stayton, P.S. RAFT-synthesized graft copolymers that enhance pH-dependent membrane destabilization and protein circulation times. J Control Release **155,** 167, 2011.
35. Al-Hassani, M.H., Garcia, J.G.N., and Gunst, S.J. Differences in Ca^{2+} mobilization by muscarinic agonists in tracheal smooth muscle. Am J Physiol Lung Cell Mol Physiol **264,** L53, 1993.
36. Gunst, S.J., Stropp, J.Q., and Flavahan, N.A. Interaction of contractile responses in canine tracheal smooth muscle. J Appl Physiol (1985) **63,** 514, 1987.
37. Gunst, S.J., and Russell, J.A. Contractile force of canine tracheal smooth muscle during continuous stretch. J Appl Physiol Respir Environ Exer Physiol **52,** 655, 1982.
38. Furnish, E.J., Brophy, C.M., Harris, V.A., *et al.* Treatment with transducible phosphopeptide analogues of the small heat shock-related protein, HSP20, after experimental subarachnoid hemorrhage: prevention and reversal of delayed decreases in cerebral perfusion. J Neurosurg **112,** 631, 2010.

Address correspondence to:
Padmini Komalavilas, PhD
Department of Surgery
Vanderbilt University Medical Center
MCN T2111, 1161 21st Avenue South
Nashville, TN 37232-2730

E-mail: padmini.komalavilas@vanderbilt.edu

Received: June 8, 2018
Accepted: August 13, 2018
Online Publication Date: October 26, 2018